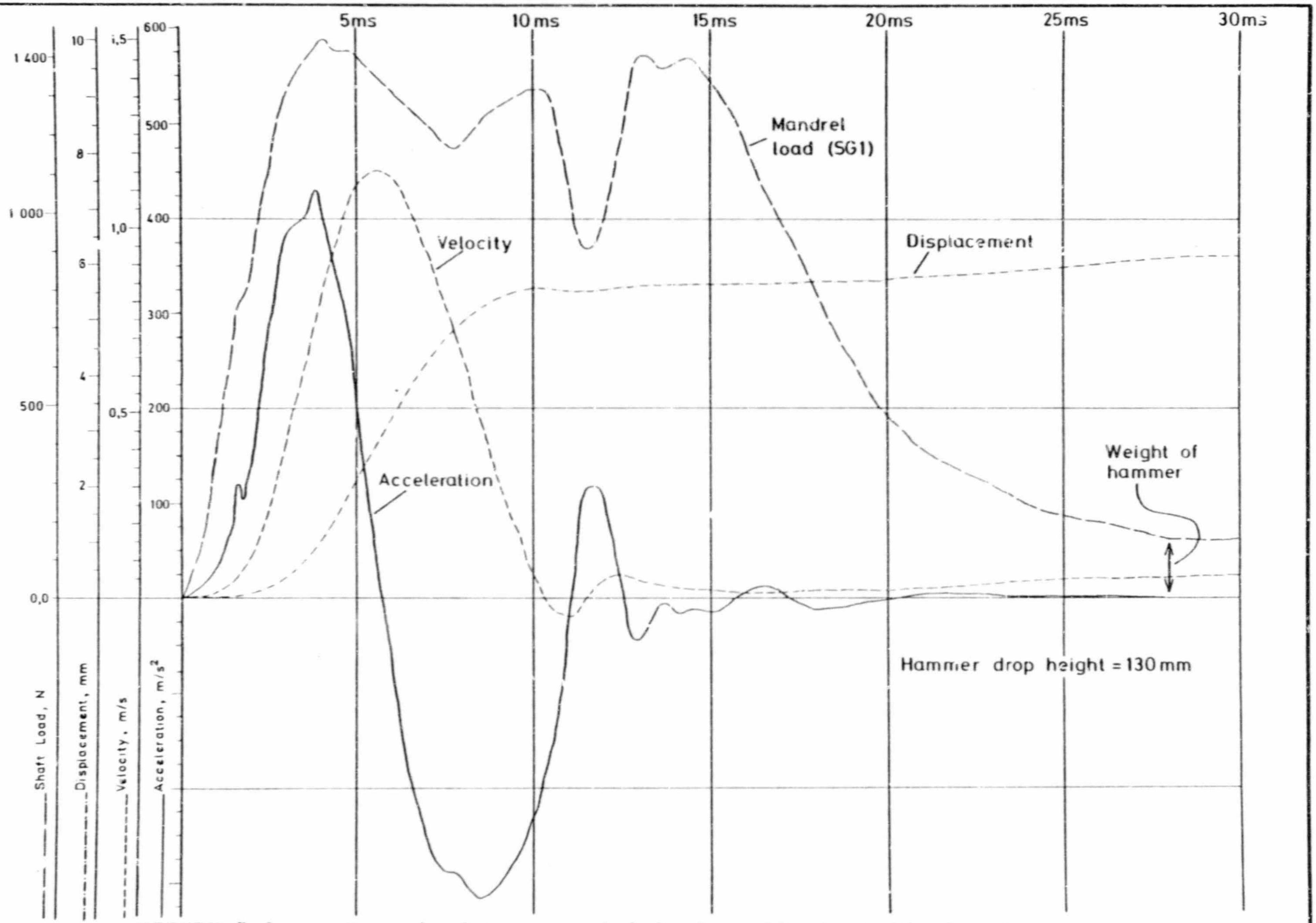

FIGURE 5.1 : Dynamic data recorded during pile installation. (Refer Plate 5.1b)

trace of the impact load developed near the head of the pile (at SG6), was similar in form to that at SG1. An example of this similarity is given in Plate 5.1d which was obtained during experiment No. 8. Of note in Plate 5.1d is the observation that the amplitude of the initial peak load recorded at the pile toe (SG1) was less than that recorded at the head of the pile (SG6) by an amount of approximately 230N. This feature was common to all the pile impacts where head and toe loads were measured. A load difference between the pile head and pile toe was also detected during the immediate post-installation static load test (see 5.2). Plate 5.1d also shows that immediately following the first load peak, the load in SG6 dropped off at a faster rate and by a greater amount than the load in SG1. About 10ms after the start of impact, the loads measured at SG1 and SG6 were approximately equal. Plate 5.2a, which gives the load trace at SG5 during test No. 8, shows a similar rapid reduction in the mandrel load at the top of the pile following the initial peak. It is suggested that load shed in friction between the grout and drive mandrel was the main cause of the measured head and toe load differences. Plates 5.1b and 5.1d also demonstrate the similarity in the form of the mandrel load and pile head acceleration traces obtained at similar depths in separate experiments. Depth related changes in the response of the model pile to impact can be seen in Plates 5.2a to 5.2d which were obtained during experiment No. 8.

Plates 5.1, a to d

Showing four oscilloscope traces of impact records on the model pile obtained during pile installation. On the photographs "A" indicates the accelerometer trace, and "L" or "SG1 or 6" the strain gauge trace.

Plate 5.1a — Test No. 9. Trace of accelerometer at pile top and strain gauge group SG1 at toe of pile. Depth of embedment approximately 744mm. Third from final hammer blow (followed by Plate 1 Dynamic).

Plate 5.1b — Test No. 9. Trace of accelerometer and SG1 as above. Depth 750mm. Pile toe penetration 5,62mm. Penultimate hammer blow (followed by Plate 2 Dynamic).

Plate 5.1c — Test No. 9. Trace of accelerometer and SG1 as above. Depth 755,62mm. Pile toe penetration 4,29mm. Final hammer blow (followed by Plate 3 Dynamic).

Note: Zero for SG1 adjusted between each of the traces shown in Plates 5.1a to 5.1c.

Plate 5.1d — Test No. 8. Trace of accelerometer and strain gauge groups SG1 and SG6. Depth approximately 760mm. Third from final hammer blow. (Note amplitude scale for the strain gauge groups is about twice that of the Test No. 9 traces.

- Horizontal scale 5ms per division.
- Vertical scale accelerometer approximately 20g per division.
- Vertical scale Test No. 9 strain gauges approximately 510N per division.
- Vertical scale Test No. 8 strain gauges approximately 255N per division.

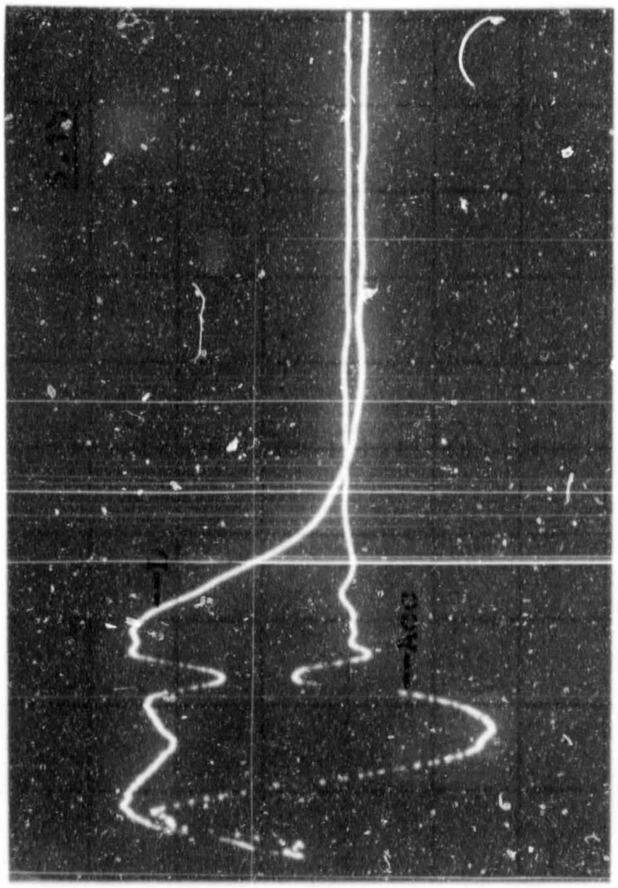

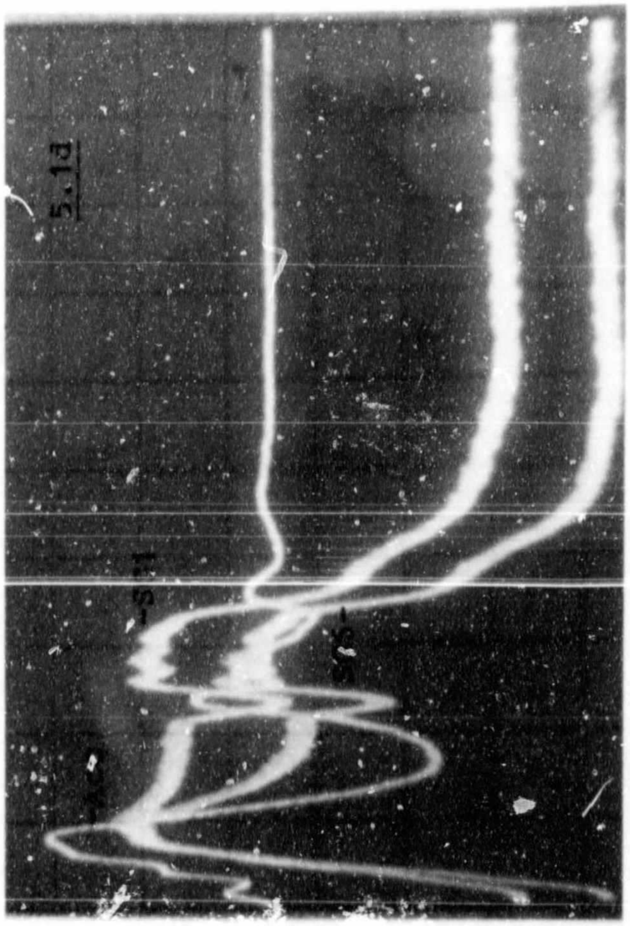
5.1d

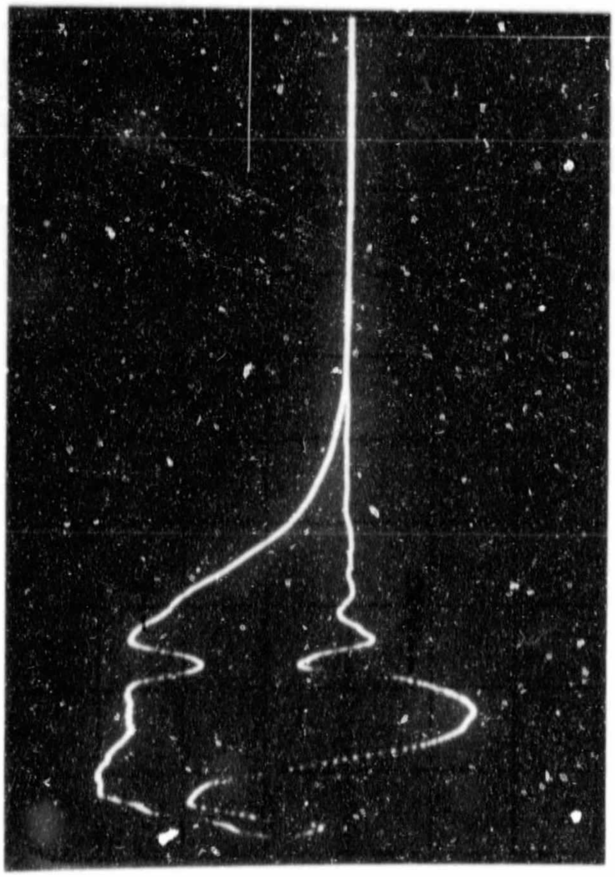

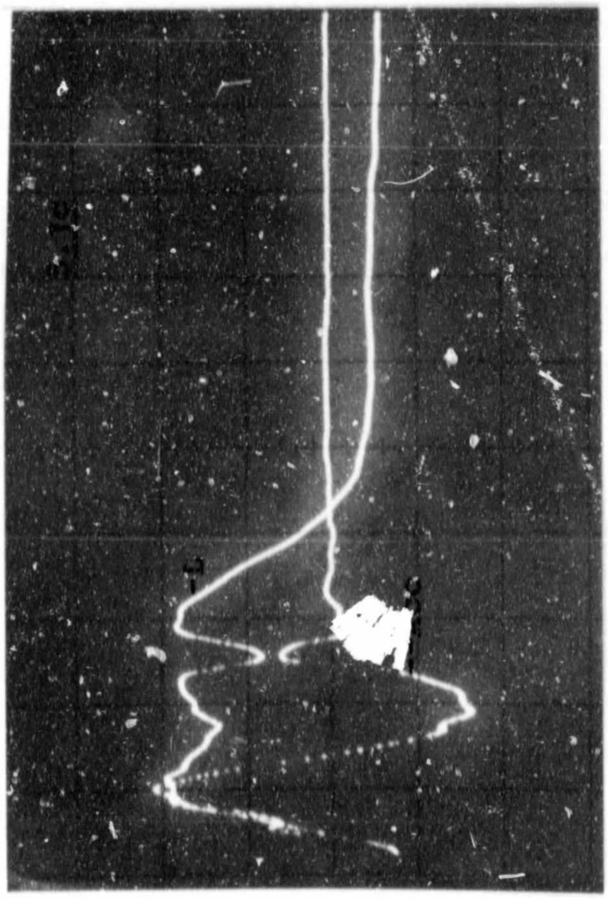

Plates 5.2, a to d

Showing four oscilloscope traces of impact records on the model pile obtained at various depths while installing the model pile during experiment No. 8.

Plate 5.2a Depth approximately 450mm. Traces of accelerometer and SG5.

Plate 5.2b Depth approximately 525mm. Traces of accelerometer and SG1.

Plate 5.2c Depth approximately 650mm. Traces of accelerometer and SG3.

Plate 5.2d Depth 766mm. Traces of accelerometer and SG1.

Note: Zero on vertical scale kept constant for accelerometer, but varied for strain gauge groups, depending on which oscilloscope channel was used.

- Horizontal scale : 5ms per division.
- Vertical scale, accelerometer approximately 20g per division.
- Vertical scale, strain gauges approximately 255N per division.

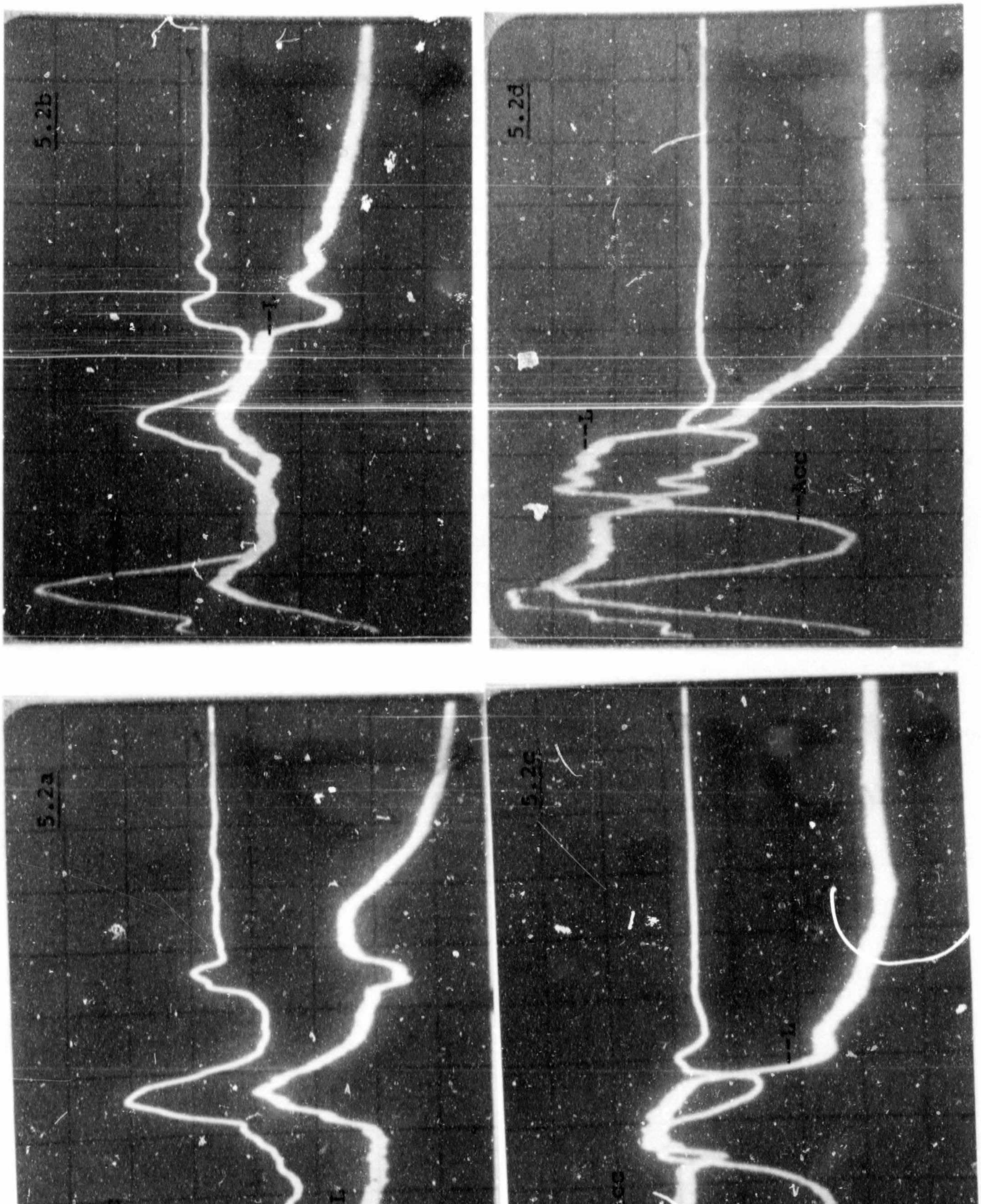
5.2b
L
5.2d
L
Acc
5.2a
Acc
L
5.2c
Acc
L

Soil movements recorded around the toe of the pile during impact installation are shown in Figures 5.2 to 5.5 (located in the rear pocket of this volume). The magnitude of the movements has been expressed in the form of contour diagrams of their horizontal (X direction) and vertical (Y direction) components of accumulated movement. In all the sand grain displacement diagrams (including Figures 5.10 to 5.17 which show movements recorded during static load testing), the grout column or pile shaft above the top of the shoe collar has been drawn as a straight line. This is a simplification as can be seen by reference to Plates 5.3, a to d. Although these diagrams were compiled from data obtained by co-ordinating individual sand grains, it is considered that the contours adequately define the loci of all grains which were subjected to similar movement components. The contour intervals in these diagrams are given in Wild A7 Stereoplotter units, where, with the instrument settings used, 1 plotter unit = 1,18 microns. As discussed in section A.4 of Appendix A, the "zero" displacement contours in fact locate the boundaries of detectable grain displacements. They more correctly correspond to the loci of sand grains with displacements of the order of 15 to 20 plotter units.

The diagrams encompass an area of approximately 330mm x 250mm true scale, around the toe and to the right of the axis of the pile respectively. A rectangular frame extending approximately 3 pile diameters to the side of the pile axis and approximately 3 pile diameters below the point of the pile shoe, has been superposed on the displacement diagrams. The frame was positioned to cover the major soil movements and therefore extends in these diagrams to only about one half a pile diameter above the top of the shoe collar. The boundary of this frame marks the edges of a 222 element rectangular grid (see Figure 6.7) which was used to estimate soil strains from the measured sand grain displacements (soil strains are discussed in Chapter 6 and Appendix D).

5.2 Static Load Testing

During the static load test conducted immediately after the installation of the pile, the peak load measured near the pile toe (at SG1, see Figure 4.3) at a low penetration rate, was 1236N. At the same time, the peak load recorded at the pile head (SGs 5 and 6), however, was 1385N. This difference suggests that some 149N of the applied load was shed in various ways along the drive mandrel. The main sources of load shedding are thought to have been due to viscous drag on the drive mandrel caused by the rising grout column, bouyancy of the partly hollow mandrel in the heavy fluid grout, and contact of the mandrel with the glass front panel via the plastic separator strip.

Five minutes after forced penetration of the pile was halted, the residual toe load (at SG1) remaining after various load redistributions including soil relaxation had occurred, was 1138N, while the load measured at the pile head was 1306N. Load losses along the drive mandrel thus rose to 168N.

Load/settlement data for the static load tests carried out on the model pile under both submerged and drained soil conditions after curing of the grout shaft are given in Tables 5.2 and 5.3, and in Figures 5.6 to 5.9. Figure 5.7 and Table 5.1 indicate the positions during these load tests at which the plate film exposures of sand movements were made (Plates 1 to 5 Static). In Figures 5.6 to 5.9, the various load increments are shown as L1, L2 ... L6, etc. L0', L6' and L12' refer to the loads applied by the reaction beam arrangement only.

After completion of the submerged load test, a period of 25 minutes was allowed for the water to drain from the sand box, though most of it had escaped after 15 minutes. The average moisture content of the sand in which the 'drained' static load test was conducted was 4,57%. It was measured using four sand samples immediately after completing the test. The average density of the moist soil was 1749 kg/m^3. The "apparent cohesion" of the sand was determined as c = 2,7 kPa.

It was assumed that at the start of the static load test on the pile in submerged sand, that all the strain gauge groups registered no load.

As can be seen in Figure 5.7, the loading procedure followed a sequence of approximately constant rate of penetration load increments. Each load increment resulted in approximately equal amounts of pile penetration: 1mm/load increment average for the test in submerged sand and 0,33mm/load increment for the test in drained sand. Load was therefore applied as necessary to achieve the desired penetration. After each load application, a minimum period of 5 minutes was allowed during which creep movements, and corresponding load reductions could occur (see Figure 5.6). Once the rate of downward creep of the pile was less than 0.02mm in 5 minutes, the next load was applied. In Figures 5.8 to 5.9, which show the load distribution down the pile shaft during the submerged and drained tests, the loads plotted, are those which remained in the pile shaft at the end of the relaxation period (residual load). In Figure 5.8, however, the shaft load distribution curve corresponding to the L5 load increment shows the peak loads achieved. The residual loads after the L5 increment were virtually the same as for the L4 increment. As can be seen in Figure 5.8, the peak load distribution curve (L5) and the residual load distribution curve (L4) are almost parallel. This feature was

It was assumed that at the start of the static load test on the pile in submerged sand, that all the strain gauge groups registered no load.

As can be seen in Figure 5.7, the loading procedure followed a sequence of approximately constant rate of penetration load increments. Each load increment resulted in approximately equal amounts of pile penetration: 1mm/load increment average for the test in submerged sand and 0,33mm/load increment for the test in drained sand. Load was therefore applied as necessary to achieve the desired penetration. After each load application, a minimum period of 5 minutes was allowed during which creep movements, and corresponding load reductions could occur (see Figure 5.6). Once the rate of downward creep of the pile was less than 0.02mm in 5 minutes, the next load was applied. In Figures 5.8 to 5.9, which show the load distribution down the pile shaft during the submerged and drained tests, the loads plotted, are those which remained in the pile shaft at the end of the relaxation period (residual load). In Figure 5.8, however, the shaft load distribution curve corresponding to the L5 load increment shows the peak loads achieved. The residual loads after the L5 increment were virtually the same as for the L4 increment. As can be seen in Figure 5.8, the peak load distribution curve (L5) and the residual load distribution curve (L4) are almost parallel. This feature was

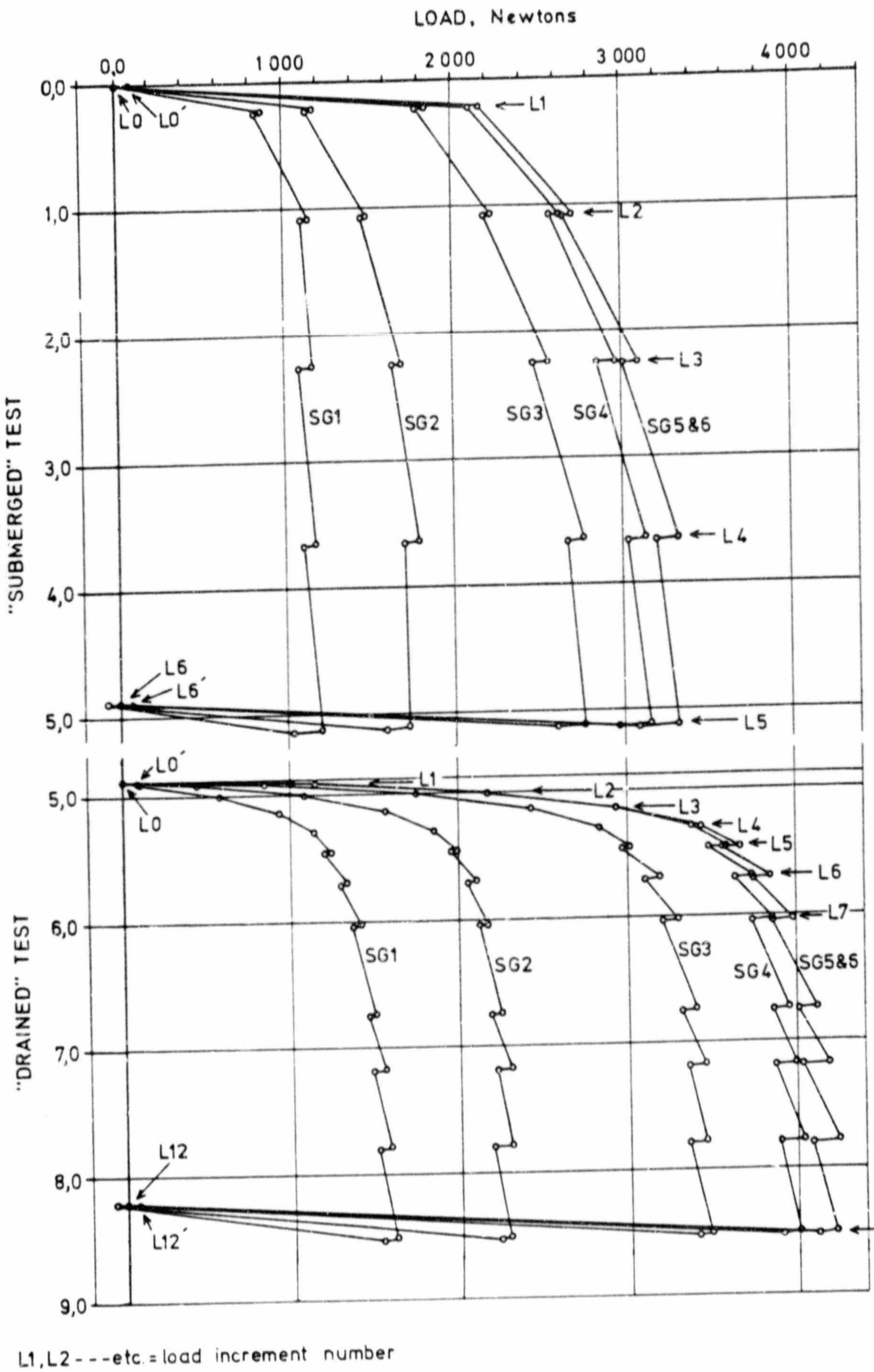

FIGURE 5.6 : Load/settlement behaviour of the model pile

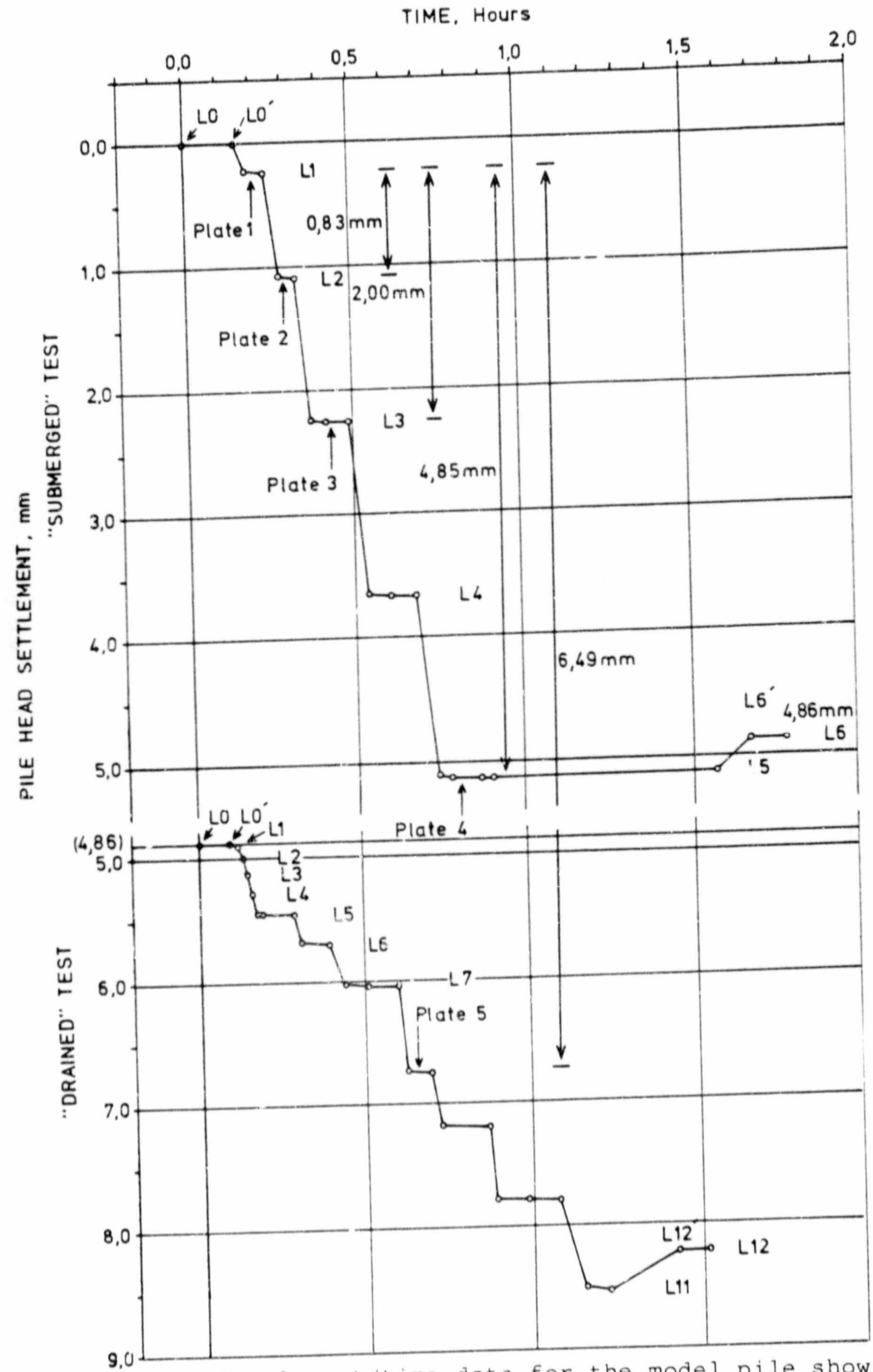

FIGURE 5.7 : Settlement/time data for the model pile showing when soil displacements were photographed

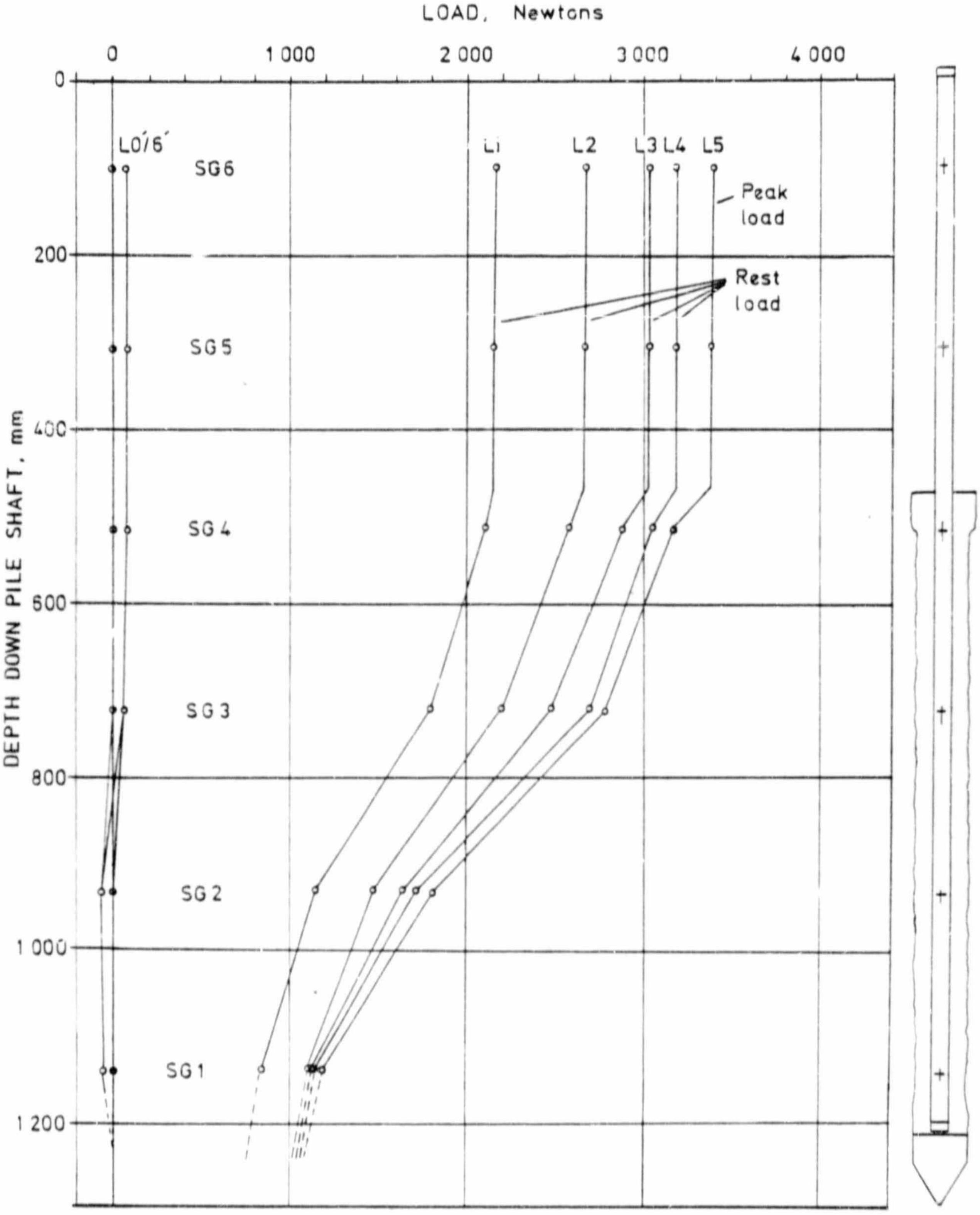

FIGURE 5.8 : Load distribution down the pile shaft during load testing of the pile in submerged sand

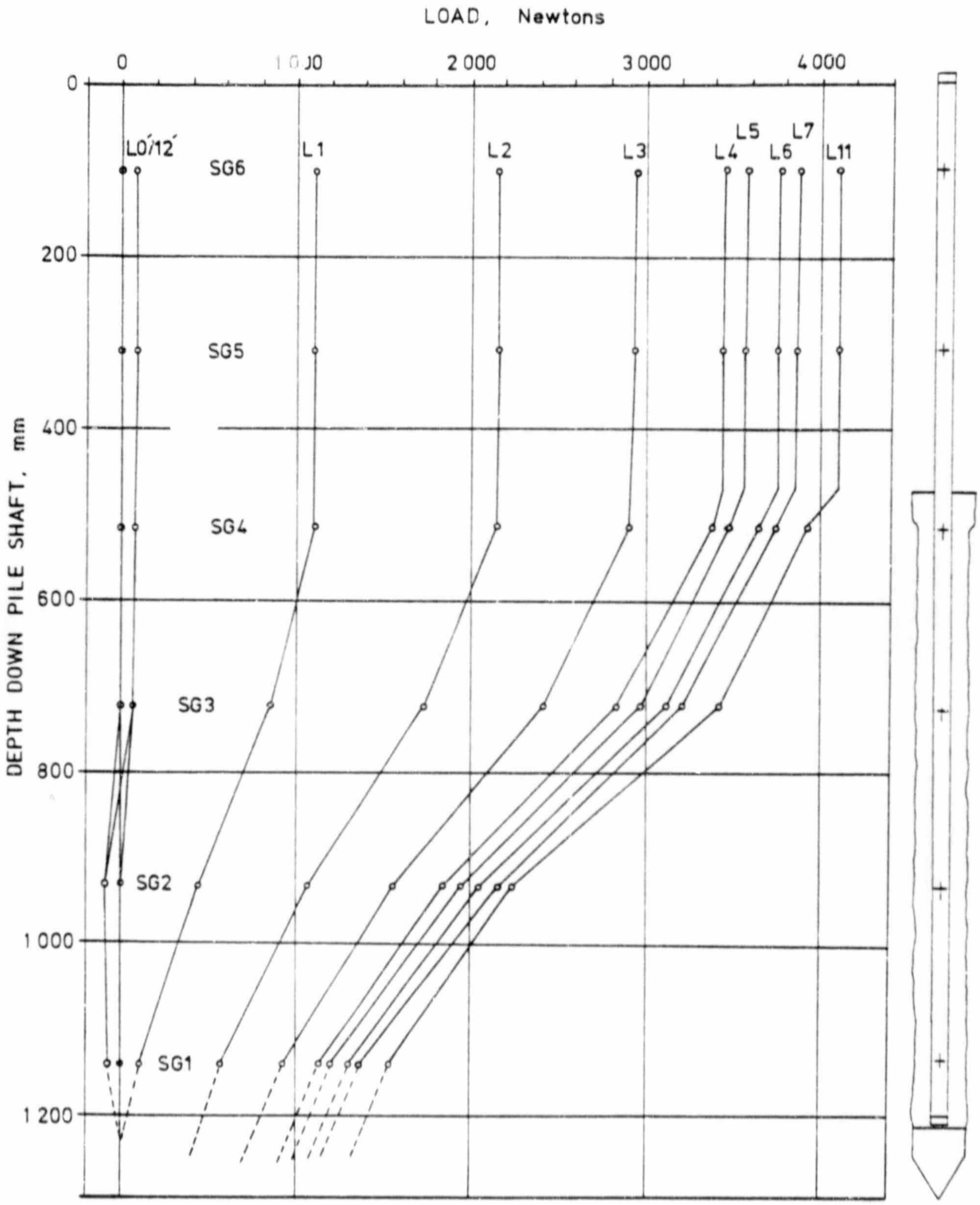

FIGURE 5.9 : Load distribution down the pile shaft during load testing of the pile in drained sand

TABLE 5.2 : Load/Settlement Records for the Static Load Test on the Pile in Submerged Sand

Load Step No.	ρ Pile Head mm	Pile Shaft Loads SG 6/5 N	SG 4 N	SG 3 N	SG 2 N	SG 1 N	Estimated Toe Load N	Plate No.
L0	0,00	0	0	0	0	0	0	-
L0'	0,04	79	77	60	0	0	0	-
L1	0,21	2228	2184	1855	1195	882	790	-
	0,23	2161	2112	1801	1147	840	750	Plate 1 (Static)
L2	1,06	2702	2642	2239	1502	1152	1060	Plate 2 (Static)
	1,07	2650	2583	2199	1472	1104	1010	-
L3	2,23	3087	2973	2569	1700	1170	1120	Plate 3 (Static)
	2,24	3010	2850	2475	1640	1086	1010	-
L4	3,63	3332	3149	2772	1796	1176	1120	-
	3,65	3198	3036	2671	1706	1104	1030	-
L5	5,08	3319	3168	2772	1724	1206	1100	Plate 4 (Static)
	5,12	3082	2977	2603	1586	1032	970	-
L6'	4,87	78	72	73	-40	-27	0	-
L6	4,86	0	0	0	-48	-36	0	-
Noise error range		SG5=±9N SG6=±9N	±12N	±12N	±12N	±12N		
Accumulated drift error at end of test		SG5= 0 SG6=±4N	±12N	0	±2N	0		

TABLE 5.3 : Load/Settlement Records for the Static Load Test on the Pile in Drained Sand

Load Step No.	ρ Pile Head mm	Pile Shaft Loads SG 6/5 N	SG 4 N	SG 3 N	SG 2 N	SG 1 N	Estimated Toe Lo[illegible] N	[illegible]ate
L0	0,00	0	0	0	-5	-26	0	-
L0'	0,00	85	82	67	4	-26	0	-
L1	0,03	1116	1114	843	445	108	0	-
	0,03	1112	1112	841	443	105	0	-
L2	0,12	2161	2152	1740	1075	576	400	-
	0,12	2155	2149	1740	1073	571	400	-
L3	0,25	2945	2914	2421	1562	930	700	-
	0,25	2933	2908	2412	1555	923	690	-
L4	0,41	3447	3391	2832	1850	1140	910	-
	0,41	3432	3381	2824	1841	1131	900	-
L5	0,57	3678	3589	3028	1994	1248	1020	-
	0,58	3570	3476	2967	1946	1200	980	-
L6	0,81	3857	3743	3197	2108	1338	1120	-
	0,83	3758	3639	3109	2048	1296	1080	-
L7	1,14	3998	3866	3305	2181	1422	1200	-
	1,16	3868	3734	3203	2120	1362	1150	-
L8	1,85	4124	3961	3406	2247	1500	1310	Plate 5 (Static)
	1,87	4018	3861	3318	2187	1452	1270	-
L9	2,29	4193	4006	3466	2301	1548	1360	-
	2,31	4041	3870	3352	2211	1476	1300	-
L10	2,90	4251	4047	3466	2301	1578	1400	-
	2,92	4089	3902	3352	2193	1506	1330	-
L11	3,63	4229	4006	3493	2289	1608	1420	-
	3,65	4123	3916	3412	2229	1530	1350	-
L12'	3,32	90	54	88	-60	-48	0	-
L12	3,31	0	-5	0	-88	-70	0	-
Noise error range		SG5=±9N SG6=±9N	±12N	±12N	±12N	±12N	-	
Accumulated drift error at end of test		SG5= 0 SG6=±9N	±20N	0	±4N	0		

TABLE 5.2 : Load/Settlement Records for the Static Load Test on the Pile in Submerged Sand

Load Step No.	ρ Pile Head mm	Pile Shaft Loads SG 6/5 N	SG 4 N	SG 3 N	SG 2 N	SG 1 N	Estimated Toe Load N	Plate No.
L0	0,00	0	0	0	0	0	0	-
L0'	0,04	79	77	60	0	0	0	-
L1	0,21	2228	2184	1855	1195	882	790	-
	0,23	2161	2112	1803	1147	840	750	Plate 1 (Static)
L2	1,06	2702	2642	2239	1502	1152	1060	Plate 2 (Static)
	1,07	2650	2583	2199	1472	1104	1010	-
L3	2,23	3087	2973	2569	1700	1170	1120	Plate 3 (Static)
	2,24	3010	2850	2475	1640	1086	1010	-
L4	3,63	3332	3149	2772	1796	1176	1120	-
	3,65	3198	3036	2671	1706	1104	1030	-
L5	5,08	3319	3168	2772	1724	1206	1100	Plate 4 (Static)
	5,12	3082	2977	2603	1586	1032	970	-
L6'	4,87	78	72	73	-40	-27	0	-
L6	4,86	0	0	0	-48	-36	0	-
Noise error range	SG5=±9N SG6=±9N	±12N	±12N	±12N	±12N			
Accumulated drift error at end of test	SG5= 0 SG6=±4N	±12N	0	±2N	0			

TABLE 5.3 : Load/Settlement Records for the Static Load Test on the Pile in Drained Sand

Load Step No.	ρ Pile Head mm	Pile Shaft Loads SG 6/5 N	SG 4 N	SG 3 N	SG 2 N	SG 1 N	Estimated Toe Load N	Plate No.
L0	0,00	0	0	0	-5	-26	0	-
L0'	0,00	85	82	67	4	-26	0	-
L1	0,03	1116	1114	843	445	108	0	-
	0,03	1112	1112	841	443	105	0	-
L2	0,12	2161	2152	1740	1075	576	400	-
	0,12	2155	2149	1740	1073	571	400	-
L3	0,25	2945	2914	2421	1562	930	700	-
	0,25	2933	2908	2412	1555	923	690	-
L4	0,41	3447	3391	2832	1850	1140	910	-
	0,41	3432	3381	2824	1841	1131	900	-
L5	0,57	3678	3589	3028	1994	1248	1020	-
	0,58	3570	3476	2967	1946	1200	980	-
L6	0,81	3857	3743	3197	2108	1338	1120	-
	0,83	3758	3639	3109	2048	1296	1080	-
L7	1,14	3998	3866	3305	2181	1422	1200	-
	1,16	3862	3734	3203	2120	1362	1150	-
L8	1,85	4124	3961	3406	2247	1500	1310	Plate 5 (Static)
	1,87	4018	3861	3318	2187	1452	1270	-
L9	2,29	4193	4006	3466	2301	1548	1360	-
	2,31	4041	3870	3352	2211	1476	1300	-
L10	2,90	4251	4047	3466	2301	1578	1400	-
	2,92	4089	3902	3352	2193	1506	1330	-
L11	3,63	4229	4006	3493	2289	1608	1420	-
	3,65	4123	3916	3412	2229	1530	1350	-
L12'	3,32	90	54	88	-60	-48	0	-
L12	3,31	0	-5	0	-88	-70	0	-
Noise error range		SG5=±9N SG6=±9N	±12N	±12N	±12N	±12N		-
Accumulated drift error at end of test		SG5= 0 SG6=±9N	±20N	0	±4N	0		

common to all the load increments. An indication of the load developed on the pile shoe has been obtained by extrapolating the load distribution curves below the lowermost strain gauge group (SG1). Once it had been established that the ultimate pile capacity had been achieved, all externally applied loads on the pile were removed, and the pile allowed to recover so that the residual settlement could be determined.

From the data given in Tables 5.2 and 5.3, it can be seen that removal of the applied loads resulted in the development of tensile loads at strain gauge positions SG1 and SG2. During the time elapsed between completion of the "submerged" test and starting the "drained" test, these tensile loads decreased.

Various aspects of the appearance of the model pile after it had been removed from the soil are shown in Plates 5.3, a to d. The rough irregular sandy surface of the grouted shaft, the smooth virtually plane surface of the pile grout where it cured against the plastic strip, and the bulbous region at the top of the pile where the grout reservoir was located, are clearly visible in these photographs. (Note: The section of measuring tape shown in Plates 5.3c and d was photographed with one edge placed against the side of the pile which was in contact with the plastic strip lying against the glass front of the sand box.)

Plates 5.3a to 5.3d: Showing various aspects of the model pile after removal from the sand box.

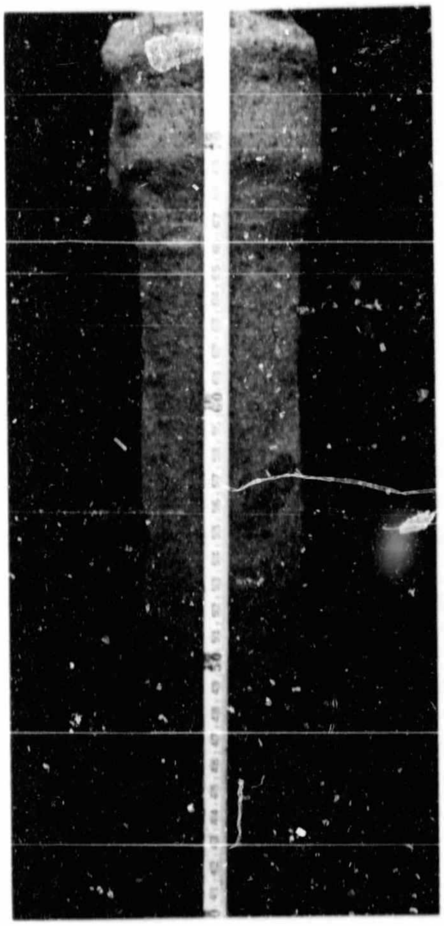

Plate 5.3a

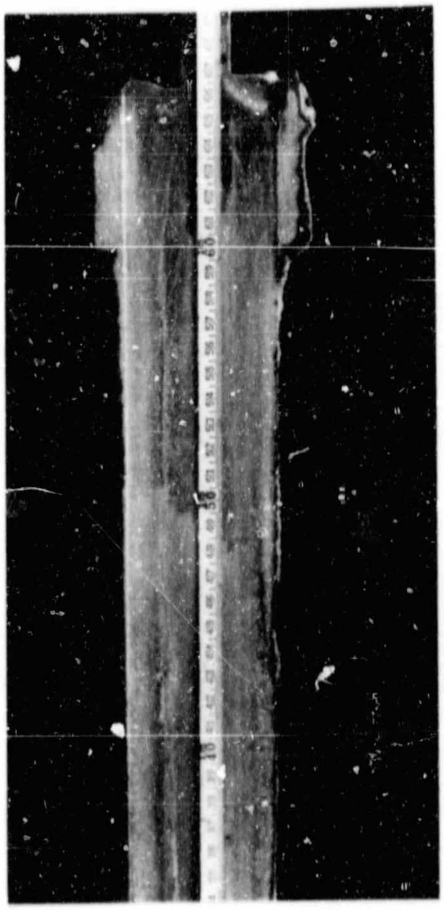

Plate 5.3b

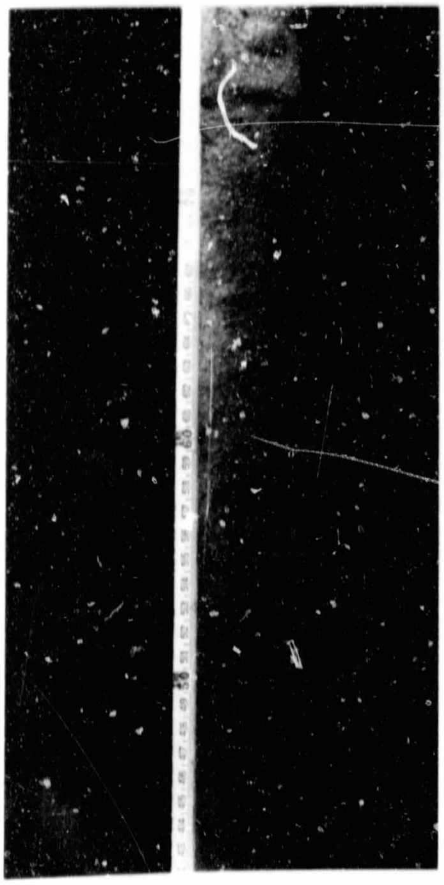

Plate 5.3c

Plate 5.3d

Measurements of the dimensions of the recovered pile indicated a radius of 42mm at the top of the pile in the grout reservoir. The radius of the shaft formed in the annulus above the pile shoe showed a roughly linear taper from 31,3mm at immediately below the reservoir bell to 27,7mm near the pile toe. The following radii were applicable to pile shaft at the various strain gauge group positions, SG1 - 27,7mm, SG2 - 29,2mm, SG3 - 30,1mm, SG4 - 42,0mm.

Despite the use of the methods described in Chapter 4 to prevent bonding of the grouted pile shaft to the glass face of the sand box, bonding did occur over some portions of pile shaft, particularly towards the pile toe. This was due mainly to leakage of grout around the plastic separating strip and grout overlapping the strip at the top of the pile where the grout reservoir had been placed during pile installation (see plate 5.3). The bond was broken during the L1 load increment of the test in submerged sand at a load of about 1800 N. Little movement of the pile head was recorded up to this load, but when the bond broke, the pile moved abruptly downwards by 0,12 mm. This portion of the load cycle has not been shown in Figure 5.6.

Figures 5.10 to 5.17 (located in the rear pocket of this volume) show the soil movements which were recorded in the basal region of the pile during the load tests. As with the sand grain displacement diagrams showing soil movements recorded during pile installation, the movements have been expressed in the form of contour diagrams of the horizontal and vertical components of accumulated movement. The contour intervals are also given in Wild A7 stereoplotter units, where 1 plotter unit = 1,18 microns. As before, the "zero" displacement contours indicate the limits of measurable soil movements and more correctly locate the loci of displacements of the order of 15 to 20 plotter units. The diagrams encompass an area of about 360mm along the pile axis and about 250mm to the one side of the pile axis.

The rectangular frame superposed on these diagrams corresponds to the boundaries of a 290 element rectangular grid (see Figure 6.20) which was used to estimate soil strains due to static loading. The grid system used for the static load tests was extended to about 3 pile diameters above the top of the shoe collar in order to obtain information on the soil behaviour along the pile shaft.

5.3 Summary

1 Of ten piles installed under controlled laboratory conditions, two were successful and one of these was selected for detailed analysis. This pile was installed to an initial depth of 760mm and to a

final depth of 792mm in an homogenous isotropic sand with an average dry density of 1673kg/m^3.

2 Pile shaft loads and head accelerations were monitored during the impact installation process. The loads given, however, are not a true measure of the soil resistance only and include friction between the glass front panel and the pile. (See Appendix E.)

3 Load tests to failure were carried out in submerged sand immediately after installation of the pile and again after the grout had cured. A third load test, carried out on the cured pile, was conducted in drained soil conditions.

4 Soil movements around the base of the pile, and load in the pile shaft were recorded during both pile installation and subsequent static load testing. The soil movement data has been presented in the form of contour diagrams of the X and Y displacement components.

6. DISCUSSION OF EXPERIMENTAL RESULTS

6.1 Impact Installation Data

The impact data, comprising mandrel load at SG1, pile head acceleration and derived pile head velocity and displacement, for the penultimate impact recorded during pile installation is shown in Figure 5.1. In this diagram, the calculated head velocity and displacement are shown to be increasing slowly from about 20ms onwards, although significant head acceleration had effectively ceased by this time. It is likely that this apparently continuing movement is due to errors incurred in measuring acceleration from a photograph of the accelerometer oscilloscope trace, and can be ignored. This is a recognised problem in the use of accelerometer data for the determination of velocity and displacement (for example, Ormondroyd et al., [1950]). The first approximately 15ms of the acceleration curve is, however, considered meaningful.

The acceleration vs. time curve in Figure 5.1 shows a fairly simple cyclical pattern of acceleration and deceleration decaying to zero, over a period of about 25ms. This pattern is similar to that expected in cases of damped impact. When expressed in terms of velocity and displacement it can be seen that the recorded pile head accelerations ceased to have a significant influence on pile head movement at about 11ms. As regards pile displacement, therefore, the impact event was effectively complete within about 11ms.

The curve showing the load induced in the drive mandrel in response to impact by the drop hammer, shows a sequence of compressive load fluctuations with peak loads being recorded at 4, 10 and 13ms, followed by gradual decay to a steady state at about 28ms. It records the resistance experienced at the pile toe, as a result of an impact induced, forced penetration of the pile into the soil as well as drag on the plastic separator strip and glass/shoe friction. Many materials are apparently more stiff at high strain rate conditions than under slow loading conditions. The loads measured in the drive mandrel during impact may therefore be underestimates of the true load. The error is, however, considered to be small.

The peak load (1450N) recorded at 4ms was probably composed in part of the ultimate dynamic bearing capacity of the submerged soil and in part of static friction against the glass front panel. When the friction corrections discussed in Appendix E are applied to this load, the soil resistance is determined as 1210N. According to the calculated displacement curve, downward movement of the pile into the soil occurred mainly within the first 11 ms following impact.

Although during this period, the measured mandrel load fluctuated in the range 1150N to 1450N, the load apparently remained at a sufficiently high level to achieve and maintain failure in the surrounding soil.

At about 11 ms after the start of impact, the mandrel load decreased abruptly to 900N. This followed slight upward movement of the pile head as indicated by a negative section on the velocity curve. Shortly thereafter the mandrel load rose again, abruptly, to 1400N, and then decayed gradually to a steady state under the static weight of the hammer (162N). Whereas soil failure was induced during the initial 11 ms at loads of between 1150N and 1450N, after the pile head rebound event, a load of 1400N developed at 13 to 15ms was apparently insufficient to cause further toe penetration.

The load difference of about 230N recorded between SG1 and SG6 in Plate 5.1d may have had some influence on the eventual skin friction capacity of the model pile. It has been suggested that this load was shed mainly into the grout column. With each hammer impact on the pile at this depth therefore, the grout was effectively "pumped" into the void following the pile shoe with a force equal to the head and toe load difference. Because it is likely that this force would have had some outward component through the grout, it is possible that the soil at the grout interface was surcharged and densified with each impact.

It is not certain why the soil resistance should have fluctuated during and after the main pile head movements. The initial stages of the load trace fluctuation may be due to interparticle friction in the soil and friction against the glass panel, changing from static to sliding friction. For some materials (see data in Gieck [1979]), the difference between static and sliding friction coefficients can be large. In the absence of other information on which this behaviour might be interpreted, it is suggested that the load peaks at 10 and 13ms indicate either rebound of the soil against the pile shoe or pore pressure effects, or a combination of the two. Possible rebound mechanisms include decompression of air voids in the submerged soil, a returning pressure wave created during initial impact and the development of temporary local quick conditions.

Mandrel load and pile head acceleration data, obtained at increasing embedment depths of the model pile during experiment No. 8, are shown as oscilloscope traces in plates 5.2 (a to d). There are distinct differences in the form of the traces obtained at the different depths. Some of these differences may be listed as follows:

(a) As the embedment depth increased, the duration of the impact event decreased from about 28ms at 450mm depth (Plate 5.2a) to about 20ms at 766mm depth (Plate 5.2d) (cf 15ms for experiment No.9 at 750mm depth of embedment [Figure 5.1 and Plate 5.1b]).

(b) Three load peaks were recorded at both 450mm and 525mm depths, but only two thereafter. Further, at the shallower depth, the two major load and acceleration peaks occurred at the same time, but did not do so at greater depths.

(c) The abrupt drop in load, with a concommitant acceleration peak previously discussed, is present in all the oscilloscope traces. At the 450mm depth, however, this event occurred towards the end of the impact period, but, at greater depths, it occurred between the two main load peaks.

(d) Supplementary peaks began to occur on the load trace at 650mm depth and became marked at the 766mm depth.

(e) At 450mm the load peaks were sharp, distinct and widely separated. As the depth increased, the peaks tended to merge and the intervening load decrease became less marked.

It is clear that depth of embedment has a significant influence on the load response of the pile/soil system to impact. A major change in the form of the oscilloscope trace of the mandrel load was recorded at between 450mm and 650mm embedment, i.e. at length to diameter ratios of between 7 and 11. This change in the response of the pile to impact, may be related to the concept of the "critical depth of embedment" suggested by Meyerhof (1976). This subject is discussed further in Chapter 7.

6.1.1 Wave Equation Analysis

The applicability of the wave equation to the model MV pile has been assessed by comparing the recorded behaviour of the model pile during the penultimate impact, with that predicted by a wave equation computer program. The program, written by colleague A.J. Bowen, was based mainly on the procedures presented by Smith (1960), and calculates for a pile and hammer system of given properties, the set per blow required to obtain a pile of specified capacity. Results obtained for pile set and pile element forces using this program have been compared with analyses given by Samson et al (1963) and Bowles (1974). Excellent correlations were obtained with the published data. For the analysis, the pile was simulated by the mass-spring system shown in Figure 6.1.

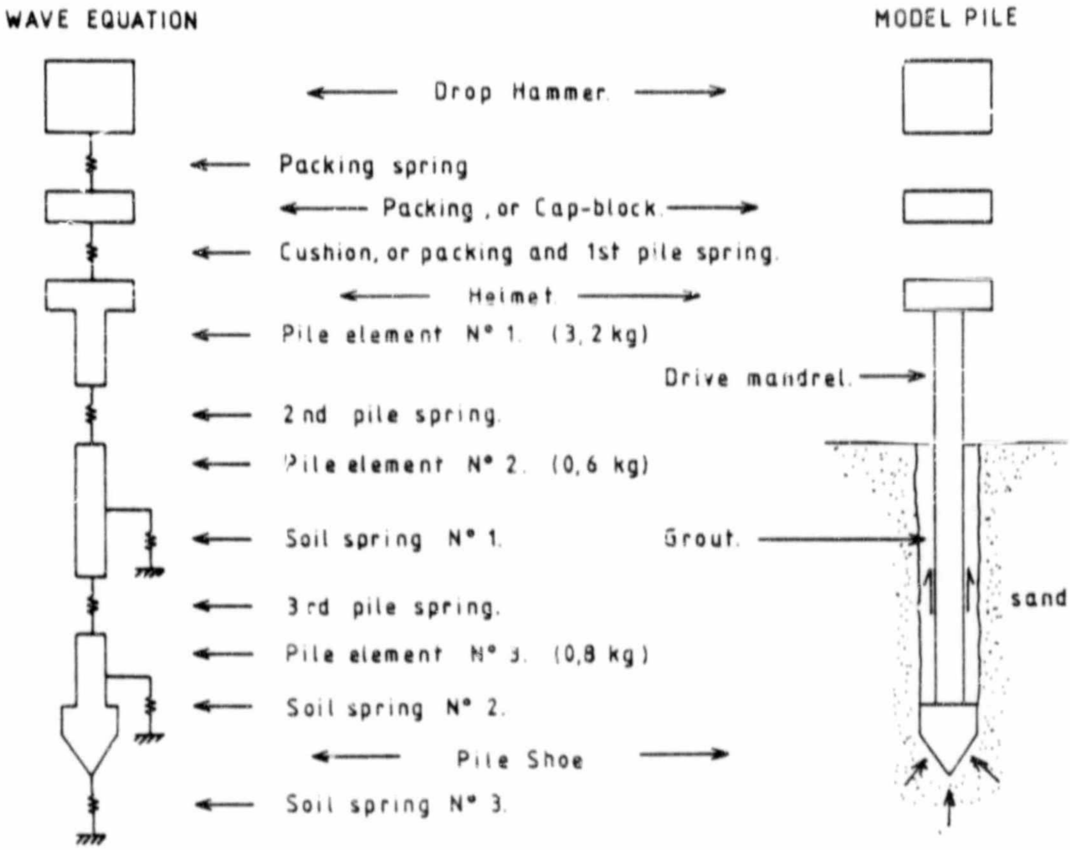

Figure 6.1 Mass/spring approximation of the model pile for the wave equation analysis

Table 6.1 lists some of the data used in the program calculations. Much of this data was measured directly, but the derivation of some of the listed values requires further explanation. In particular, only measured uncorrected loads have been used in the analysis since these were the loads experienced by the pile.

Table 6.1 : Data used in the Wave Equation Analysis

No.	Item	Quantity	Units	How obtained
1	Mass of hammer	16,5	kg	Measured
2	Mass of packing	0,5	kg	Measured
3	Mass of pile elements			
	(i) Head	3,2	kg	Measured
	(ii) Mandrel	0,35	kg	Measured
	(iii) Toe - case 1	0,71	kg	Measured
	- case 2	1,1	kg	Calculated
4	Stiffness of pile elements	65 000	kN/mm	Measured by strain gauges
5	Stiffness of packing	5,65	kN/mm	Measured
6	Stiffness of cushion	1 000 000	kN/mm	Assumed high value
7	Co-efficient of restitution packing	0,25		Measured by falling steel ball
8	Co-efficient of restitution cushion	0,55		Normal value for steel
9	Quake at pile toe	1,0	mm	See text
10	Side damping co-efficient	0,1	ms/mm	See text
11	Point damping co-efficient	0,23	ms/mm	See text
12	Pile capacity - case 1	1306	kN	See Chapter 5.2
	- case 2	2412	kN	See text
13	Percentage load on tip - case 1	87	%	See text
	case 2	93,5	%	See text

In Table 6.1, two cases are given for the data for items 3 (iii), 12 and 13. These two cases have been considered in an attempt to estimate the influence of 3-dimensional effects on the wave equation analyses. For these items, case 1 applies to data for the semi-circular model pile as installed, while the case 2 data applies to a theoretical model pile as if it were complete and circular. For item 12, case 2, it has been assumed that had the model pile been circular, the resistance measured at the pile toe would have been twice that of the half pile. The percentage load on the pile tip for item 13, case 2, was estimated on the assumption that the frictional load shed along the mandrel would have been the same (168N) for both the half pile and for the theoretical circular pile.

Smith's (op cit) damping co-efficients, Js and Jp, provide . method by which the strength of the soil around the pile toe and shaft under static loading conditions, is adjusted upwards to compensate for the greater apparent strength of - soil when it is rapidly loaded (see Figure 6.2b). Smith's equation for expressing the increase of soil strength with loading rate is given in terms of pile element ve   ty as:

$$Ru_{dyn} = Ru_{stat} (1 + J.V)$$

where Ru = resistance on the pile element

J = damping co-efficient (point or side of pile)

V = pile element velocity

In Figure 5.1, Ru_{dyn} was measured as 1450N. Ru_{stat} (= 1138N) was obtained from the load test carried out immediately after the pile had been installed (see Chapter 5). The peak element velocity shown in Figure 5.1 was 1,17m/s. On substituting these data into Smith's equation, the required value of the point damping coefficient was calculated as 0.23ms/mm. Following common practice the value selected for the side damping coefficient was approximately 1/3 Jp. These values do not change if Ru_{dyn} and Ru_{stat} are corrected for friction on the glass panel.

The pile load measured during the static load test which followed immediately after the installation of the pile was 1306N. Of this, 1133N or 87%, was carried on the

Smith's (op cit) damping co-efficients, Js and Jp, provide a method by which the strength of the soil around the pile toe and shaft under static loading conditions, is adjusted upwards to compensate for the greater apparent strength of a soil when it is rapidly loaded (see Figure 6.2b). Smith's equation for expressing the increase of soil strength with loading rate is given in terms of pile element velocity as:

$$Ru_{dyn} = Ru_{stat} (1 + J.V)$$

where Ru = resistance on the pile element

J = damping co-efficient (point or side of pile)

V = pile element velocity

In Figure 5.1, Ru_{dyn} was measured as 1450N. Ru_{stat} (= 1138N) was obtained from the load test carried out immediately after the pile had been installed (see Chapter 5). The peak element velocity shown in Figure 5.1 was 1,17m/s. On substituting these data into Smith's equation, the required value of the point damping coefficient was calculated as 0.23ms/mm. Following common practice the value selected for the side damping coefficient was approximately 1/3 Jp. These values do not change if Ru_{dyn} and Ru_{stat} are corrected for friction on the glass panel.

The pile load measured during the static load test which followed immediately after the installation of the pile was 1306N. Of this, 1138N or 87%, was carried on the